Materials Today Communications 49 (2025) 113708

Contents lists available at ScienceDirect

Materials Today Communications

journal homepage: www.elsevier.com/locate/mtcomm

TOPSIS optimization of solvent modulated pressureless submicron sintered silver for power electronics

Xinyue Wang [a], Haixue Chen [a], Zhoudong Yang [a], Wenting Liu [a], Guoqi Zhang [b], Jing Zhang [c], Chuangtong Chen [d], Pan Liu [a,e,*]

[a] College of Intelligent Robotics and Advanced Manufacturing, Fudan University, Shanghai 200433, China
[b] Department of Microelectronics, Delft University of Technology, Delft 2628 CD, the Netherlands
[c] Heraeus Materials Technology Shanghai Ltd., Shanghai 201108, China
[d] Flexible 3D System Integration Laboratory, SANKEN, Osaka University, Osaka, Japan
[e] Research Institute of Fudan University, Ningbo, Zhejiang Province 315336, China

ARTICLE INFO

Keywords:
Sintering
Joining
Metal matrix composites (MMC)
Power electronic packaging
Aging

ABSTRACT

Pressureless sintered silver pastes composed of submicron particles represent a promising, cost-effective interconnect solution for power electronics. While epoxy additives are often introduced to modify solvent behavior and enhance mechanical integrity, they can simultaneously degrade electrical and thermal performance, leading to critical trade-offs. In this work, five custom-formulated pastes with varying epoxy contents (0–4 wt%) and two commercial benchmarks were systematically evaluated in terms of shear strength, resistivity, thermal conductivity, and coefficient of thermal expansion (CTE). To optimize across multiple criteria, the Technique for Order Preference by Similarity to Ideal Solution (TOPSIS) was employed. The paste containing 2 wt% epoxy achieved the highest composite score, offering a favorable combination of mechanical, thermal, and electrical properties. Long-term reliability was further validated through high-temperature storage and thermal cycling tests. These results highlight that epoxy modulation, when integrated with an optimization framework, offers a viable strategy for tailoring high-performance, reliable sintered silver joints for next-generation power electronic packaging.

1. Introduction

The rapid development of power electronics has brought forth increasing demands for interconnect materials capable of withstanding extreme thermal and mechanical stresses [1,2]. Such materials serve as critical components in high-power, high-temperature applications, where both performance and long-term reliability are paramount [2–5]. Among various candidates, sintered silver has emerged as a promising lead-free alternative to traditional lead-based solders, meeting the stringent requirements of next-generation power packaging while complying with global environmental regulations [6,7]. In particular, pressureless sintered silver joints offer distinct advantages, including excellent process compatibility, outstanding thermal conductivity, low electrical resistivity, and superior mechanical robustness [8–10]. Moreover, the adoption of micron-scale silver for pressureless sintering has recently emerged as a practical strategy to reduce manufacturing costs, addressing both environmental and economic considerations in high-power electronic assembly [11].

However, to fully harness these benefits, it is necessary to further investigate the role of solvent modulation in reinforcing bonding strength and improving joint stability [11–16], along with the use of advanced algorithms for multi-criteria decision-making to systematically optimize material formulations. Epoxy additives, frequently introduced to modify paste rheology and enhance adhesion, play a complex role in determining the final properties of the sintered joint [17–19]. Although such additives improve processability, their impact on the thermal, mechanical, and electrical performance of the resulting joints remains underexplored, particularly with respect to balancing competing property requirements [20–23].

To address this challenge, we proposed an optimization strategy that integrates epoxy modulation with a multi-criteria decision-making approach. Specifically, the Technique for Order Preference by Similarity to an Ideal Solution (TOPSIS) was selected to systematically rank paste formulations based on their proximity to an ideal performance profile.

* Corresponding author at: College of Intelligent Robotics and Advanced Manufacturing, Fudan University, Shanghai 200433, China.
E-mail address: panliu@fudan.edu.cn (P. Liu).

https://doi.org/10.1016/j.mtcomm.2025.113708
Received 6 May 2025; Received in revised form 11 August 2025; Accepted 30 August 2025
Available online 1 September 2025

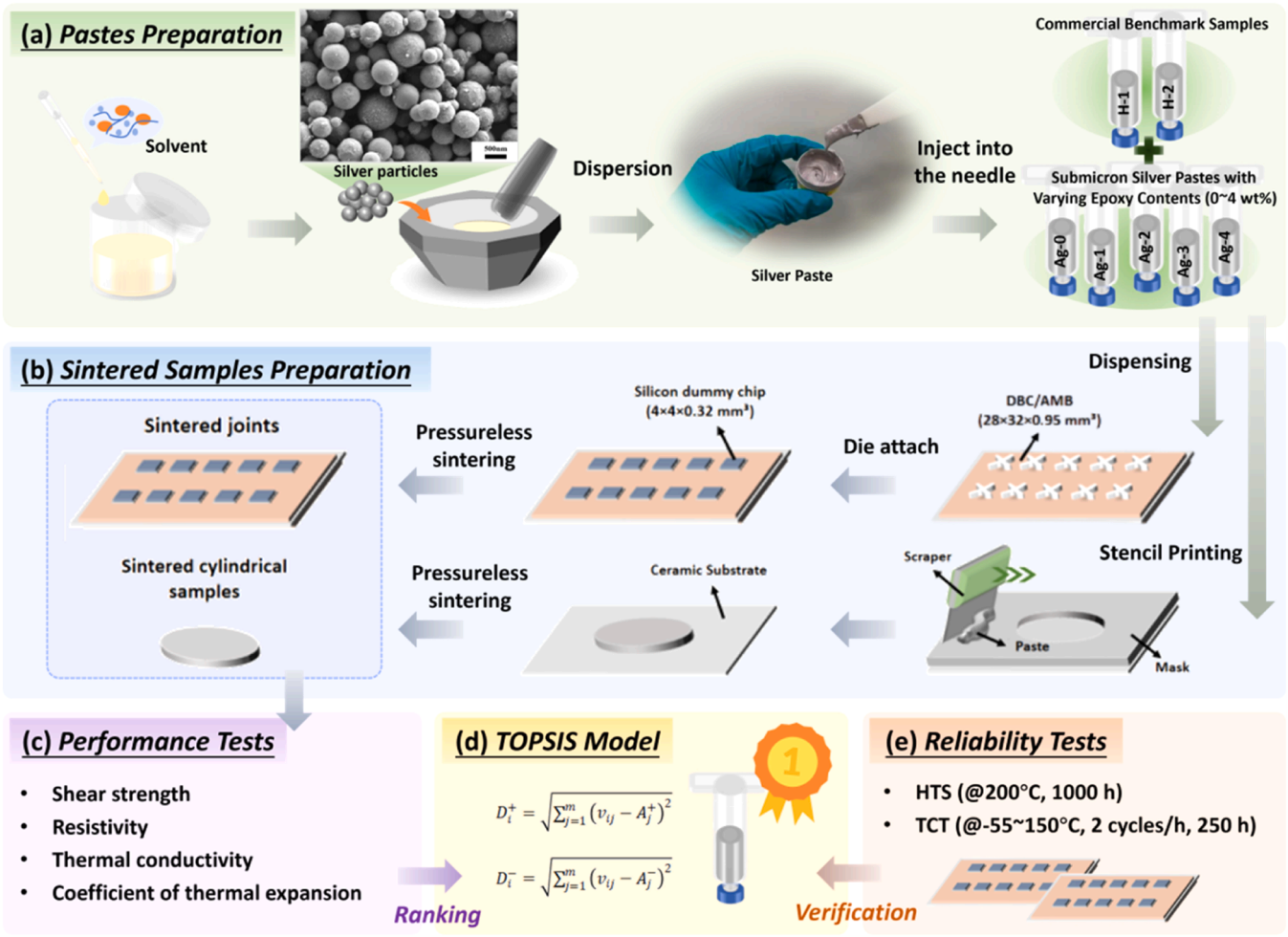

Fig. 1. The technical roadmap of this work.

Compared with more complex algorithms, TOPSIS offers notable advantages in terms of simplicity, transparency, and suitability for rapid screening in materials design [20–23]. The TOPSIS methodology involves the following key steps [24–27]:

1. Min-Max Normalization of the Decision Matrix: Each criterion value was normalized to eliminate unit inconsistency using the equation:

$$r_{ij} = \frac{x_{ij} - x_j^{\min}}{x_j^{\max} - x_j^{\min}} \tag{1}$$

where x_{ij} is the original value of the *j-th* criterion for the *i-th* alternative.

2. Weighted Normalized Decision Matrix: The normalized values were multiplied by their respective weights (w_j) to calculate the weighted normalized matrix:

$$v_{ij} = w_j \cdot r_{ij} \tag{2}$$

3. Determine the Ideal Best (A^+) and Worst (A^-) Solutions:

$$A^+ = \{\max(v_{ij}) | j \in \text{benefit}\} \cup \{\min(v_{ij}) | j \in \text{cost}\} \tag{3}$$

$$A^- = \{\min(v_{ij}) | j \in \text{benefit} \cup \{\max(v_{ij}) | j \in \text{cost}\} \tag{4}$$

4. Distance to the Ideal Best (D_i^+) and Worst (D_i^-): The Euclidean distance to A^+ and A^- was computed using:

$$D_i^+ = \sqrt{\sum_{j=1}^{m}\left(v_{ij} - A_j^+\right)^2} \tag{5}$$

$$D_i^- = \sqrt{\sum_{j=1}^{m}\left(v_{ij} - A_j^-\right)^2} \tag{6}$$

5. Relative Closeness to the Ideal Solution (C_i): The TOPSIS score (C_i) was calculated as:

$$C_i = \frac{D_i^-}{D_i^+ + D_i^-} \tag{7}$$

The technical framework of this work is illustrated in Fig. 1. To systematically investigate the influence of epoxy content on the performance of pressureless sintered silver joints, five submicron silver pastes (Ag-0 to Ag-4) were formulated, each containing 85 wt% silver and 0–4 wt% epoxy in 1 wt% increments. In addition, two commercial pastes (H-1 and H-2) were included as benchmarks for comparison. These formulations were designed to explore the performance trade-offs introduced by solvent modulation across key metrics, including shear strength, electrical resistivity, thermal conductivity, and coefficient of thermal expansion (CTE). Each property was experimentally characterized, normalized, and assigned equal weighting within the TOPSIS evaluation model to determine the optimal formulation. This integrated methodology enabled a comprehensive assessment of performance

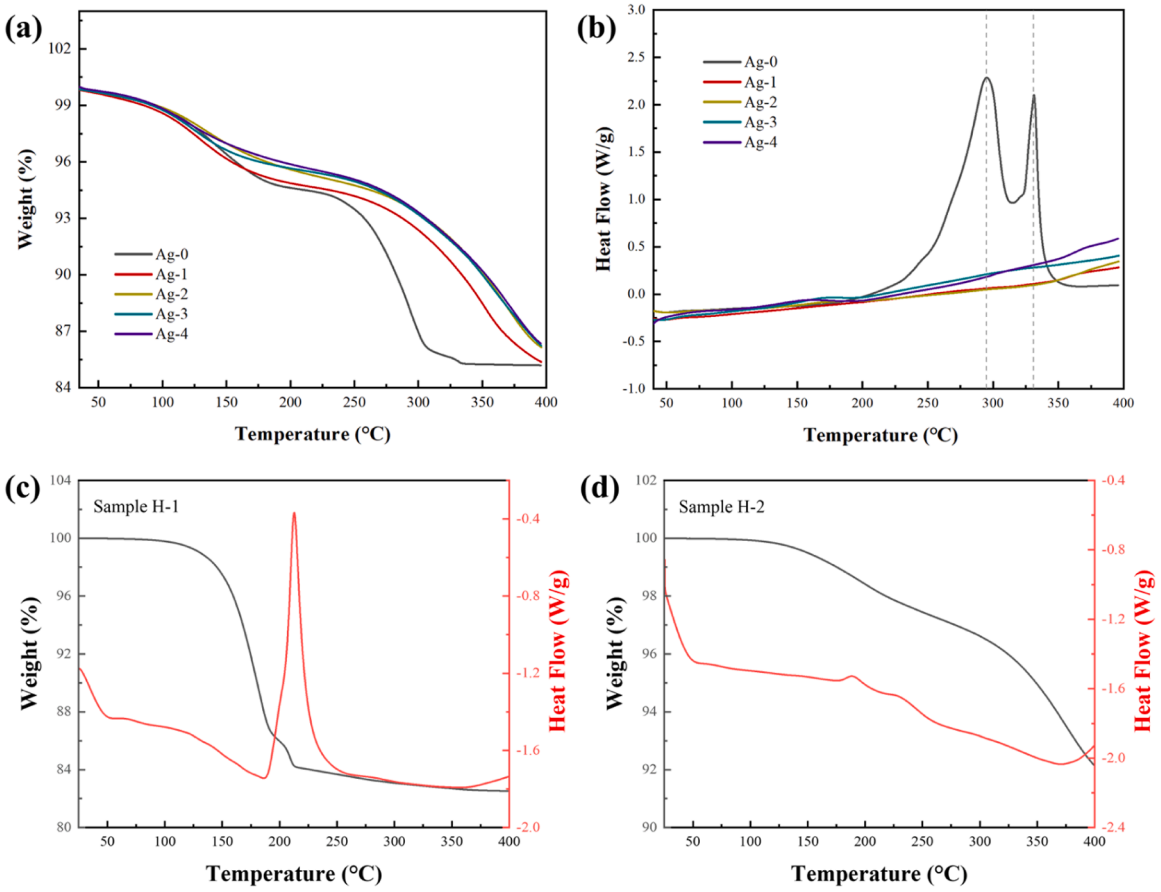

Fig. 2. Thermogravimetric and differential scanning calorimetry (DSC) analysis of silver pastes: (a) TG curves of Ag-0–Ag-4; (b) DSC curves of Ag-0–Ag-4; (c) TG-DSC curve of commercial paste H-1; (d) TG-DSC curve of commercial paste H-2.

trade-offs and provided a robust basis for material selection. To further validate the TOPSIS outcomes, the top-ranked pastes were subjected to high-temperature storage (HTS) and thermal cycling (TCT) tests to assess long-term reliability. The results confirm the effectiveness of combining epoxy modulation with multi-objective optimization for the development of reliable and cost-efficient sintered silver joints in power electronics.

2. Materials and methods

2.1. Sintering pastes preparation

The five designed epoxy-based submicron pressureless sintering silver pastes were primarily composed of submicron silver particles and organic solvents. The spherical silver particles (Ningbo Guangbo Nano New Materials Co., Ltd.) exhibited an average particle size of 500 nm, as illustrated in Fig. 1a. The organic system includes polyethylene glycol (PEG), terpineol (T), bisphenol A epoxy resin (YD), methyltetrahydrophthalic anhydride (WNY-1021), and 2-ethyl-4-methylimidazole (EMI-2,4). PEG and terpineol, combined in a 1:2 mass ratio, served as dispersants to stabilize the silver particles and enhance paste rheology. The epoxy constituents, comprising YD resin and WNY-1021 curing agent, were integrated in a 10:9 mass ratio. Additionally, EMI-2,4 was incorporated as a curing accelerator at a 10:1 ratio relative to WNY-1021 to expedite curing.

To prepare these pastes, 85 wt% silver particles were mixed with organic solvents. Dispersants (T and PEG) were incorporated and stirred for over 10 min to ensure uniformity. Subsequently, the epoxy components and silver particles were introduced, and the mixture was homogenized utilizing a planetary mixer at 1000 rpm for 3 min.

2.2. Sintered samples preparation

The prepared sintering pastes were applied to substrates using a 350PC Smart dispenser (Musashi Engineering Inc.), while dummy silicon chips with 100 nm silver plating on the backside were positioned using a Datacon 2200 evo die bonder. Sintering was conducted in a Binder M115 furnace under a nitrogen atmosphere. This systematic process ensured uniform paste distribution and reliable bonding, providing a robust foundation for performance evaluation. Additionally, cylindrical samples (diameter 12.7 mm, thickness 1–1.3 mm) were simultaneously prepared by screen printing for subsequent resistivity, thermal conductivity and CTE tests.

To minimize the differences in process parameters and isolate the effects of formulation, all in-house pastes (Ag-0 to Ag-4) were sintered using a unified curve (Fig. 3a), which was established through thermogravimetric differential scanning calorimetry (TG-DSC) utilizing a TA SDT-Q600 analyzer and preliminary experiments. Five silver pastes (Ag-0 to Ag-4) were heated from room temperature to 400 °C, with results illustrated in Fig. 2a and b. For Ag-0, the TG curve demonstrated rapid weight loss due to the decomposition and volatilization of T and PEG. Beyond 300 °C, weight stabilized, indicating complete decomposition of organic components. The heat flow curve (Fig. 2b) presented exothermic peaks at 295 °C and 331 °C, corresponding to the volatilization of T and PEG. In contrast, the TG-DSC curves of the epoxy-added pastes (Ag-1 to Ag-4) displayed more gradual weight reductions, with slower rates correlating with increased epoxy content. This suggested higher organic residue retention during sintering. Heat flow curves exhibited enhanced exothermic activity proportional to epoxy content, reflecting stronger curing reactions. For Ag-1 to Ag-4, the weight gradually stabilized close to 85 % by 400 °C, but with a more extended transition region compared

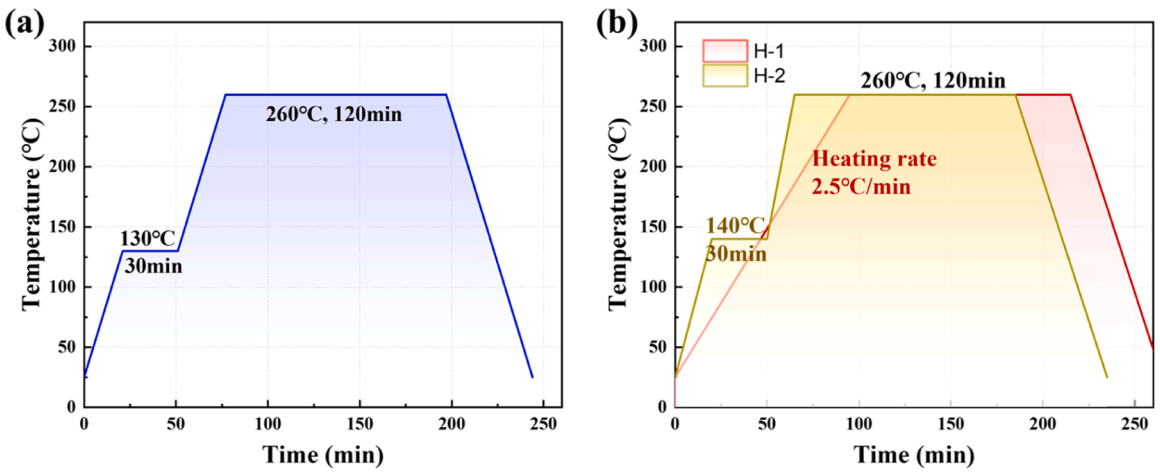

Fig. 3. Sintering profiles of silver pastes: (a) heating profile for in-house prepared Ag-0~Ag-4 pastes; (b) heating profiles for commercial pastes H-1 and H-2, based on the manufacturers' datasheets.

to Ag-0, due to the prolonged decomposition and curing of epoxy components. Based on TG-DSC analysis, a pre-drying temperature of 130 °C for 30 min and a sintering dwell temperature of 260 °C for 120 min were selected for efficient decomposition and strong bonding. The sintering temperature of 260 °C was selected based on the exothermic curing behavior of epoxy-containing pastes observed between 220 °C and 280 °C. The pre-drying step at 130 °C aimed to remove volatile solvents (PEG and terpineol), as indicated by TGA data, ensuring consistent solvent removal and minimizing porosity during sintering. It is worth noting that the sintering parameters of each configured paste may be further optimized individually to enhance performance, which will be the subject of future investigation.

In contrast, commercial reference pastes H-1 and H-2 were sintered according to their respective datasheet-recommended heating profiles (Fig. 3b). Both employed a final sintering stage of 260 °C for 120 min, while differed in ramp rates and preheating plateaus. TG-DSC analysis (Fig. 2c~d) indicated that H-2 samples retained more thermally stable organics after curing, which may influence their thermal, electrical, and mechanical behavior.

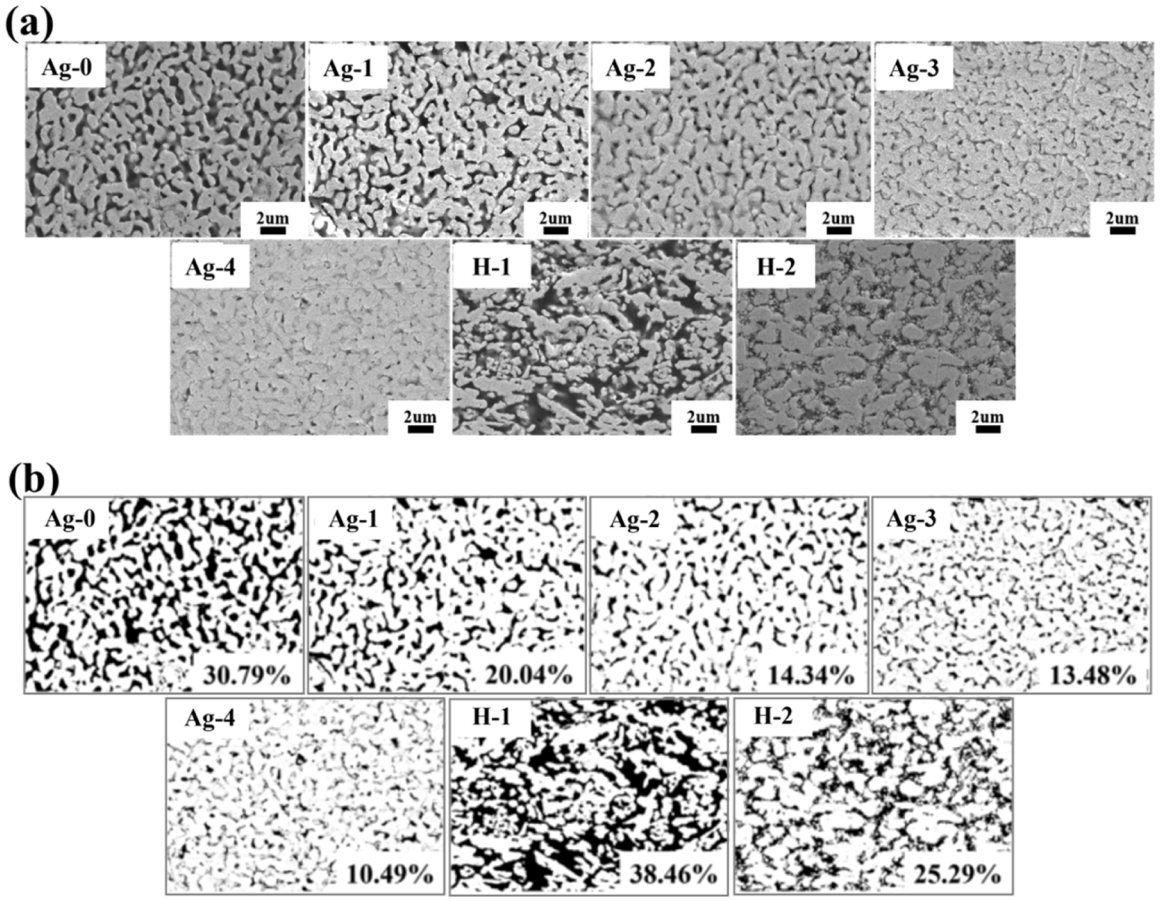

Fig. 4. (a) Cross-sectional micromorphology SEM images and (b) porosity of pressureless sintered silver joints.

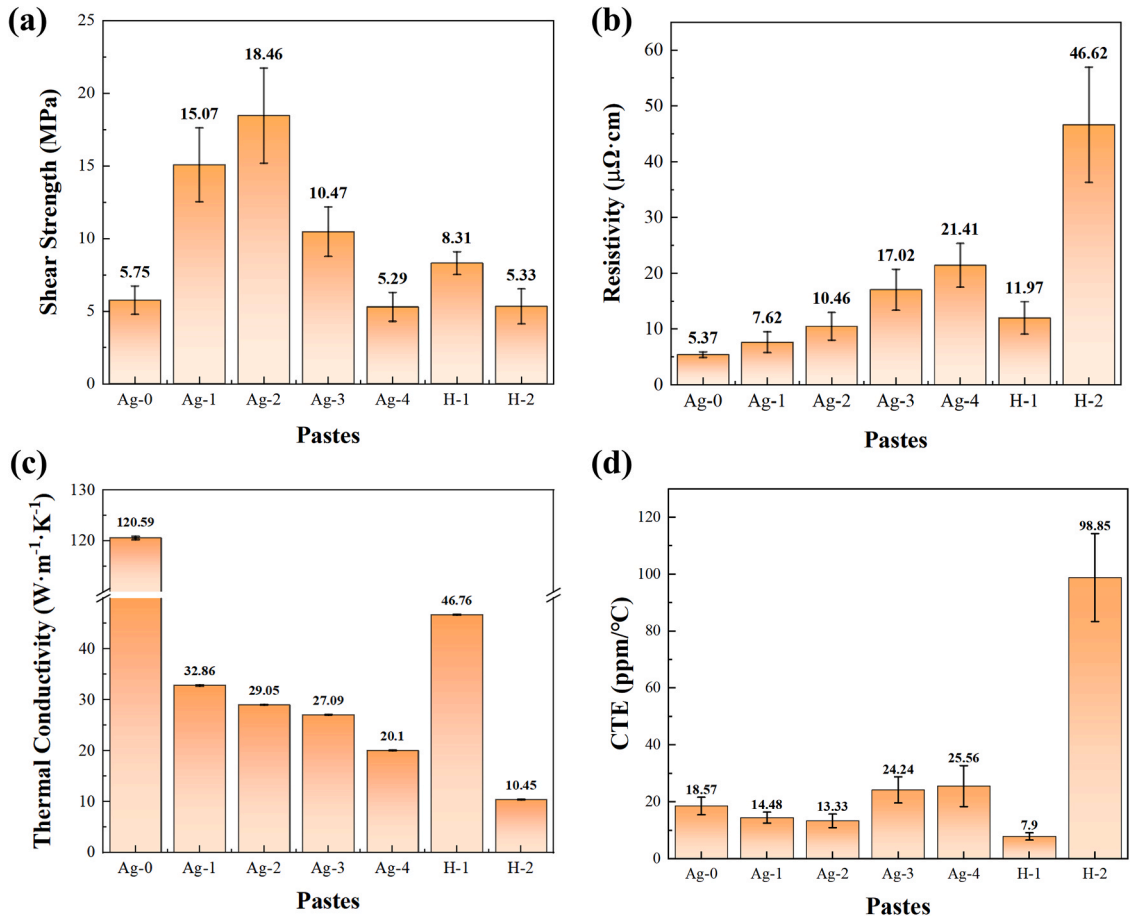

Fig. 5. (a) Shear strength, (b) electrical resistivity, (c) thermal conductivity, and (d) thermal expansion coefficient (at 200°C) of different pressureless sintered silver joints.

2.3. Performance tests

Performance tests of sintered joints in this work includes the microstructure porosity, shear strength, electrical resistivity, thermal conductivity, CTE, and reliability testing. The microstructure of the sintered samples was observed using scanning electron microscopy (SEM, ZEISS Gemini 300). Porosity was quantified from cross-sectional SEM images using ImageJ V1.8.0, where binarized black regions corresponded to pore areas. Shear strength was measured on direct bonded copper (DBC) substrates at room temperature using a Dage 4000Plus bond tester. Electrical resistivity was determined at room temperature with an RTS-11 four-probe tester, and thermal conductivity was evaluated using an LFA 467 laser flash analyzer. The coefficient of thermal expansion (CTE) was measured at 200 °C using a TMA/SDTA 2 + thermal mechanical analyzer.

Reliability testing comprised high-temperature storage (HTS) and thermal cycling test (TCT) to simulate the extreme thermal and mechanical stresses in power module operation. HTS was performed on DBC substrates per JESD22-A103E at 200°C, with shear strength recorded over aging time. TCT was conducted on active metal brazing (AMB) substrates per JESD22-A104E, cycling between −55 °C and 150 °C at 2 cycles/h for up to 500 cycles. The substrate selection aimed to replicate the characteristic stress conditions of each test—DBC for stable isothermal exposure, and AMB (Active Metal Brazed) substrates for superior mechanical integrity under repeated thermal shock. Each reliability group consisted of 24 parallel samples to ensure statistical robustness.

3. Results and discussion

3.1. Microstructure analysis

Firstly, to enhance the understanding of the behavior of epoxy-based pressureless sintered silver joints under operational conditions, cross-sectional microstructures of five sintered joints and two commercial samples were analyzed. Fig. 4a presents cross-sectional SEM images of each joint. With increasing epoxy content, the joints exhibited progressively denser and more uniform microstructures, mainly due to residual epoxy filling pores and promoting particle bridging during sintering. Contrary to the typical concern that epoxy might retain solvents and cause porosity, in our process, the pre-drying effectively removed volatile solvents. The remaining low-content epoxy (Ag-1 and Ag-2) acted as a binder, enhancing particle-particle bonding and neck growth, resulting in reduced porosity and improved interface quality. At excessive epoxy content (Ag-3 and Ag-4), higher organic residue retention inhibited particle contact and limited sintering neck formation, thereby compromising joint quality and reliability. It is also noted that while the overall silver backbone appears similar across Ag-0 to Ag-4, the internal porosity and interfacial contact maybe differ markedly due to epoxy-assisted densification. Commercial samples displayed distinct microstructures: H-1 exhibited a flaky silver particle structure with pronounced porosity, while H-2 showed multi-sized spherical particles with better densification.

Porosity analysis was presented in Fig. 3b. The Ag-0 joint exhibited an interconnected porosity of 30.79 %, while increased epoxy content reduced porosity and led to isolated pores. The lowest porosity (10.49 %) was observed in Ag-4. However, excessive epoxy impeded

Table 1
TOPSIS evaluation results.

Paste	Shear Strength @DBC (MPa)	Resistivity (μΩ·cm)	Thermal Conductivity (W/m·K)	CTE @200°C (ppm/°C)	TOPSIS Score	Rank
Ag−0	5.75 ± 0.98	5.37 ± 0.51	120.59 ± 0.31	18.57 ± 3.13	0.632	3
Ag−1	15.07 ± 2.55	7.62 ± 1.87	32.86 ± 0.11	14.48 ± 1.95	0.645	2
Ag−2	18.46 ± 3.27	10.46 ± 2.48	29.05 ± 0.04	13.33 ± 2.40	0.660	1
Ag−3	10.47 ± 1.71	17.02 ± 3.68	27.09 ± 0.02	24.24 ± 4.67	0.516	5
Ag−4	5.29 ± 0.99	21.41 ± 3.93	20.1 ± 0.02	25.56 ± 7.24	0.417	6
H−1	8.31 ± 0.79	11.97 ± 2.90	46.76 ± 0.05	7.90 ± 1.33	0.569	4
H−2	5.33 ± 1.20	46.62 ± 10.33	10.45 ± 0.03	98.85 ± 15.45	0.002	7

further particle contact and densification, underscoring the need to optimize epoxy content to balance porosity reduction and interconnect quality. For the commercial benchmarks, H-1 and H-2 showed porosities of 38.46 % and 25.29 %, respectively. These values are consistent with their observed microstructural features, with H-1 exhibiting flaky particles with large voids and H-2 displaying better-packed spherical particles. Although their initial processing differed from our in-house protocol, both were ultimately cured at 260 °C for 120 min, ensuring comparability in the final microstructure evaluation. These findings emphasized the importance of designing appropriate epoxy content for high-density and reliable pressureless sintered silver layers.

3.2. Properties analysis

Next, the mechanical, electrical and thermal properties, and CTE of the sintered silver joints were systematically evaluated.

As shown in Fig. 5a, the bonding strength of the sintered joints varied notably with epoxy content. Compared to the epoxy-free Ag-0 joints, which demonstrated an average shear strength of 5.75 ± 0.98 MPa, the addition of epoxy substantially improved enhanced joint strength. Specifically, the Ag-1 and Ag-2 joints, exhibited shear strengths of 15.07 ± 2.55 MPa and 18.46 ± 3.27 MPa, corresponding to enhancements of 1.62 × and 2.21 × , respectively. Conversely, excessive epoxy additions reduced strength, with Ag-3 and Ag-4 showing 10.47 ± 1.71 MPa and 5.29 ± 0.99 MPa, respectively, likely due to inhibited silver particle bonding caused by residual organics. Commercial samples H-1 and H-2 demonstrated shear strengths of 8.31 ± 0.79 MPa and 5.33 ± 1.20 MPa, respectively, notably lower than Ag-1 and Ag-2, primarily due to their higher porosity levels.

The electrical resistivity results (Fig. 5b) reveal a gradual increase with rising epoxy content. Ag-0 recorded a resistivity at 5.37 ± 0.51 μΩ·cm, while Ag-1 and Ag-2, with minimal epoxy additions, showed moderate increases to 7.62 ± 1.87 μΩ·cm and 10.46 ± 2.48 μΩ·cm, respectively. However, Ag-3 and Ag-4 experienced substantial resistivity increases, reaching 17.02 ± 3.68 μΩ·cm and 21.41 ± 3.93 μΩ·cm, respectively. This trend is attributed to polymer residues impeding electron pathways. While Ag-1 and Ag-2 retained adequate conductivity for interconnections, the excessive epoxy severely degraded electrical performance.

A similar downward trend was also observed in thermal conductivity (Fig. 5c). Ag-0 exhibited a thermal conductivity of 120.59 ± 0.31 $W{\cdot}m^{-1}{\cdot}K^{-1}$, while epoxy-based samples showed reduced conductivity due to the lower thermal conductivity of epoxy. Ag-1, Ag-2, and Ag-3 maintained relatively high values of 32.86 ± 0.11 $W{\cdot}m^{-1}{\cdot}K^{-1}$, 29.05 ± 0.04 $W{\cdot}m^{-1}{\cdot}K^{-1}$, and 27.09 ± 0.02 $W{\cdot}m^{-1}{\cdot}K^{-1}$, respectively. In contrast, Ag-4 showed declines to 20.1 ± 0.02 $W{\cdot}m^{-1}{\cdot}K^{-1}$, due to insulating epoxy layers increasing thermal resistance.

In contrast to conductivity trends, the coefficient of thermal expansion (CTE) at 200°C (Fig. 5d) showed a non-linear response to epoxy content. The epoxy-containing samples exhibited lower CTE values than Ag-0 and H-2, with Ag-1 and Ag-2 showing 14.48 ± 1.95 ppm/°C and 13.33 ± 2.40 ppm/°C, respectively. Such reduction was attributed to the combined effects of lower porosity, the mechanical constraint provided by the cured epoxy network, and enhanced particle-particle and particle-epoxy bonding, which together stabilize the thermal expansion behavior of the joints. However, excess epoxy in Ag-3 and Ag-4 led to elevated CTE values of 24.24 ± 4.67 ppm/°C and 25.56 ± 7.24 ppm/°C, respectively, as epoxy's higher expansion coefficient compared to silver dominated. Commercial samples H-1 and H-2 exhibited the lowest (7.90 ± 1.33 ppm/°C) and highest (98.85 ± 15.45 ppm/°C) CTE values, respectively. Although the porosity level influences CTE, the exceptionally high value for H-2 is likely associated with the presence of a polymer-rich matrix in its formulation. DSC-TGA analysis suggests that substantial polymeric residues remain after sintering at 260 °C. The inherently high CTE of such a polymer phase, combined with its presumably greater volume fraction in H-2 compared with H-1, may offset the effect of its lower porosity and lead to the highest overall CTE among all samples. These observations highlight the importance of optimizing epoxy content to balance porosity reduction and thermal expansion control.

Based on the aforementioned performance evaluation of various samples, notable variability was observed across the four tested properties. While certain formulations demonstrated superior shear strength or thermal conductivity, others excelled in resistivity or CTE. This indicates that the addition of epoxy resin brings limitations. The increased epoxy content inevitably leads to higher electrical resistivity and reduced thermal conductivity, due to the presence of polymeric residues within the sintered structure. In addition, the complex curing dynamics of epoxy can cause variability in joint properties under different processing conditions. As such, optimizing the epoxy content remains a delicate balance between enhancing mechanical strength and preserving desirable functional properties, which must be carefully considered for the target application requirements.

3.3. TOPSIS evaluation and weighting considerations

Subsequently, to address this complexity and identify the optimal formulation, a TOPSIS method was employed [28–31]. Four key performance metrics were considered: shear strength (benefit), resistivity (cost), thermal conductivity (benefit), and CTE (cost).

The results of the TOPSIS calculation, including the performance metrics, TOPSIS scores, and rankings, are summarized in Table 1. The paste Ag-2 achieved the highest score (0.660), demonstrating optimal balance across the criteria, followed by Ag-1 (0.645). Conversely, the commercial paste H-2 exhibited the lowest score, reflecting its suboptimal performance. The rankings provide a comprehensive basis for selecting the most suitable paste formulation for high-reliability applications.

It should be noted that although the addition of epoxy inevitably reduces thermal conductivity compared to pure silver joints (from 120.59 $W{\cdot}m^{-1}{\cdot}K^{-1}$ for Ag-0–29.05 $W{\cdot}m^{-1}{\cdot}K^{-1}$ for Ag-2), this level remains comparable or higher than conventional die-attach solder alloys and conductive adhesives commonly applied in high-temperature power modules. At the same time, moderate epoxy addition (e.g., 2 wt% in Ag-2) notably enhanced shear strength by improving particle bonding and mitigating brittle fracture, as also supported by previous studies [6, 32–34]. Therefore, Ag-2 is considered to offer an optimal balance between mechanical integrity and acceptable thermal performance, whereas excessive epoxy additions would cause unacceptable thermal degradation.

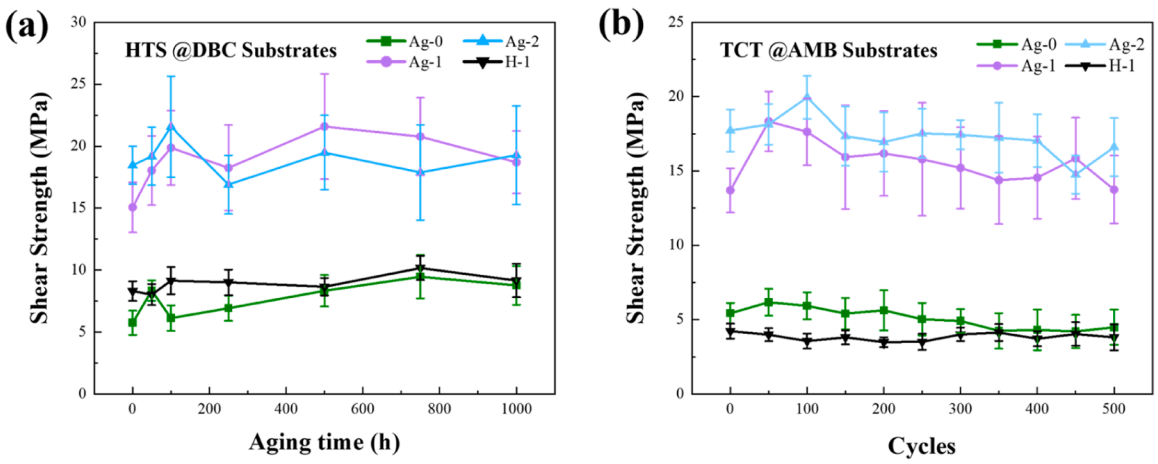

Fig. 6. Shear strength of sintered silver joints (a) after different high temperature aging times; (b) after different thermal cycles.

In this work, equal weights (wj=0.25) were assigned to all four criteria to avoid subjective bias and ensure an objective, first-level screening of overall material performance. The equal-weighting approach provides a neutral baseline for comparative evaluation across different formulations, while certain properties such as shear strength or thermal conductivity may take precedence over others (e.g., CTE) in practical applications. Depending on the specific requirements of various applications (e.g., automotive, aerospace, or industrial power modules), different weighting schemes or minimum performance thresholds for individual metrics may applied. Incorporating sensitivity analyses or developing application-specific weighted models would further enhance the robustness of the decision-making process, followed by future work for the optimization framework refinement.

3.4. Reliability analysis

Finally, to evaluate the reliability of the selected sintered silver pastes, the top-performing samples (Ag-2, Ag-1, and Ag-0) and benchmark paste (H-1) were subjected to HTS and TCT.

As shown in Fig. 6a, the HTS results revealed distinctions in long-term stability among the tested joints. Ag-1 and Ag-2 exhibited excellent stability, with no observable degradation in shear strength after 1000 h. In the early aging stage (0–100 h), their shear strengths increased by 28.5 % and 16.9 %, reaching 19.87 MPa and 21.58 MPa, respectively. This improvement was attributed to the curing of residual epoxy components at high temperatures, enhancing interparticle bonding. Over time, epoxy decomposition and volatilization, combined with silver particle neck growth, sustained high shear strength. After 1000 h, Ag-1 and Ag-2 retained shear strengths of 18.70 MPa and 19.28 MPa, respectively, maintaining considerably higher performance than Ag-0 and H-1, whose strengths degraded below 10 MPa.

Fig. 6b presents the TCT results, showing the shear strength evolution over 500 thermal cycles. Ag-1 and Ag-2 maintained high shear strengths with minor fluctuations, retaining 13.75 MPa and 16.61 MPa, respectively, after 500 cycles. In contrast, Ag-0 and H-1 exhibited a slight decline in performance fluctuation, with the shear strength stabilized at approximately 5 MPa after aging for more than 300 cycles. The superior performance of Ag-1 and Ag-2 was attributed to their low CTE values, which reduced mismatch stress between the sintered layer and substrate during thermal cycling, preserving the mechanical integrity of the joints.

The reliability results demonstrated that the epoxy-based sintered silver pastes Ag-1 and Ag-2 exhibited excellent performance in both HTS and TCT. Both samples maintained high shear strength, with minimal degradation, highlighting their mechanical robustness and suitability for power semiconductor applications. These findings validated the effectiveness of the TOPSIS optimization method, which integrated key performance indicators to identify the best formulations. Ag-1 and Ag-2 consistently outperformed other samples in reliability tests, aligning with their high TOPSIS scores.

4. Conclusions

This study proposed an optimization strategy for pressureless sintered silver joints by modulating epoxy content and employing multi-criteria decision analysis. Among all formulations, the 2 wt% epoxy-modified paste (Ag-2) achieved the most favorable balance across mechanical strength, electrical resistivity, thermal conductivity, and long-term reliability. The integration of the TOPSIS method enabled rapid and quantitative evaluation of performance trade-offs under an equal-weighting scheme, identifying Ag-2 as the optimal formulation. The addition of epoxy evidently enhanced the mechanical performance, reduced porosity and conductivity, and introduced potential variability due to curing dynamics. These insights offer a practical basis for the design of next-generation interconnect materials in power electronic packaging, where cost, performance, and reliability should be considered comprehensively.

CRediT authorship contribution statement

Chuangtong Chen: Writing – review & editing, Supervision, Resources. **Wenting Liu:** Investigation, Data curation. **Zhoudong Yang:** Visualization, Formal analysis. **Jing Zhang:** Writing – review & editing, Supervision, Resources, Conceptualization. **Guoqi Zhang:** Writing – review & editing, Supervision. **Haixue Chen:** Writing – original draft, Investigation, Formal analysis, Data curation. **Xinyue Wang:** Writing – original draft, Methodology, Investigation, Formal analysis, Data curation. **Pan Liu:** Writing – review & editing, Supervision, Project administration, Methodology, Funding acquisition, Conceptualization.

Declaration of Competing Interest

The authors declare that they have no known competing financial interests or personal relationships that could have appeared to influence the work reported in this paper.

Acknowledgments

In this work, the authors would like to thank National Natural Science Foundation of China (Grant 62304051), Shanghai Science & Technology Commission (Grant 24500790700), Doctoral Student Program of the Young Elite Scientists Sponsorship Program by CAST (2024),

and Shanghai SiC Power Devices Engineering & Technology Research Center (19DZ2253400) for funding this research. Many thanks to Chat Generative Pre-Trained Transformer (ChatGPT, OpanAI) for language help.

Data Availability

Data will be made available on request.

References

[1] H. Lee, V. Smet, R. Tummala, A review of SiC power module packaging technologies: challenges, advances, and emerging issues, IEEE J. Emerg. Sel. Top. Power Electron. 8 (1) (2020) 239–255, https://doi.org/10.1109/jestpe.2019.2951801.

[2] V.R. Manikam, C.Kuan Yew, Die attach materials for high temperature applications: a review, IEEE Trans. Compon. Packag. Manuf. Technol. 1 (4) (2011) 457–478, https://doi.org/10.1109/tcpmt.2010.2100432.

[3] B.P. Singh, K.R. Choudhury, S. Norrga, K. Kostov, H.P. Nee, Ieee, Analysis of the Performance of Different Packaging Technologies of SiC Power Modules during Power Cycling Test, 29th International Workshop on Thermal Investigations of ICs and Systems,(THERMINIC), Budapest, HUNGARY, 2023.

[4] S.H. Chen, J. Wells, T. Raner, T. Moore, L. Stuart, C. LaBarbera, Y.L. Zheng, K. Lodoe, B. Boncella, T. Muraharasetty, J. Skojec, Ieee, Highly Reliable Silver Sintering Joints for Power Module Application, IEEE Applied Power Electronics Conference and Exposition (APEC), Ieee, Orlando, FL, 2023, pp. 2575-2580.

[5] F. Forndran, J. Heilmann, M. Leicht, B. Wunderle, Physics-of-failure based lifetime modelling for SiC based automotive power modules using rate- and temperature-dependent modelling of sintered silver, Microelectron. Reliab. 163 (2024), https://doi.org/10.1016/j.microrel.2024.115550.

[6] H. Zhang, J. Minter, N.-C. Lee, A brief review on High-Temperature, Pb-Free Die-Attach materials, J. Electron. Mater. 48 (1) (2018) 201–210, https://doi.org/10.1007/s11664-018-6707-6.

[7] R. Khazaka, L. Mendizabal, D. Henry, Review on joint shear strength of Nano-Silver paste and its Long-Term high temperature reliability, J. Electron. Mater. 43 (7) (2014) 2459–2466, https://doi.org/10.1007/s11664-014-3202-6.

[8] Z. Cui, Q. Jia, H. Zhang, Y. Wang, L. Ma, G. Zou, F. Guo, Review on shear strength and reliability of nanoparticle sintered joints for power electronics packaging, J. Electron. Mater. 53 (6) (2024) 2703–2726, https://doi.org/10.1007/s11664-024-10970-9.

[9] P. Zhang, X. Jiang, P. Yuan, H. Yan, D. Yang, Silver nanopaste: synthesis, reinforcements and application, Int. J. Heat. Mass Transf. 127 (2018) 1048–1069, https://doi.org/10.1016/j.ijheatmasstransfer.2018.06.083.

[10] W. Liu, R. An, C. Wang, Z. Zheng, Y. Tian, R. Xu, Z. Wang, Recent progress in rapid sintering of nanosilver for electronics applications, Micromachines 9 (7) (2018), https://doi.org/10.3390/mi9070346.

[11] M. Wang, H. Zhang, X. Du, H. Yan, W. Hu, Y. Mei, Characterization of multiple commercial sintered-silver pastes as die attachment for power electronics packaging: materials, processing, and properties, IEEE J. Emerg. Sel. Top. Power Electron. 13 (1) (2025) 892–903, https://doi.org/10.1109/jestpe.2024.3495815.

[12] H. Yang, Study on the preparation process and sintering performance of doped nano-silver paste, Rev. Adv. Mater. Sci. 61 (1) (2022) 969–976, https://doi.org/10.1515/rams-2022-0273.

[13] K. Sugiura, T. Iwashige, K. Tsuruta, C.T. Chen, S. Nagao, T. Sugahara, K. Suganuma, Thermal stability improvement of sintered ag die-attach materials by addition of transition metal compound particles, Appl. Phys. Lett. 114 (16) (2019) 4, https://doi.org/10.1063/1.5094073.

[14] K. Li, Y. Liu, J. Zhang, Z. Pan, N. Xiao, Ieee, AgCu bimetallic sintering for power electronic packaging, 23rd International Conference on Electronic Packaging Technology (ICEPT), Ieee, Dalian, PEOPLES R CHINA, 2022.

[15] Y.W. Dai, Z. Zan, S. Zhao, Y.N. Li, F. Qin, Shearing fracture toughness enhancement for sintered silver with nickel coated multiwall carbon nanotubes additive, Eng. Fract. Mech. 260 (2022) 14, https://doi.org/10.1016/j.engfracmech.2021.108181.

[16] V. Smet, M. Jamal, A. Mathewson, K.M. Razeeb, Ieee, Thermocompression Bonding of Ag-MWCNTs Nanocomposite Films as an Alternative Die-Attach Solution for High Temperature Packaging of SiC Devices, 62nd IEEE Electronic Components and Technology Conference (ECTC), Ieee, San Diego, CA, 2012, pp. 231-237.

[17] M. Arifin, N. Wivanius, N.F. Prebianto, Ieee, Epoxy Adhesive as Die Attach Material in Semiconductor Packaging: A Review, International Conference on Applied Engineering (ICAE), Ieee, Batam, INDONESIA, 2018.

[18] Z. Sun, J. Li, M. Yu, M. Kathaperumal, C.-P. Wong, A review of the thermal conductivity of silver-epoxy nanocomposites as encapsulation material for packaging applications, Chem. Eng. J. 446 (2022), https://doi.org/10.1016/j.cej.2022.137319.

[19] S.J. Han, S. Lee, K.S. Jang, Epoxy-Based copper (Cu) sintering pastes for enhanced bonding strength and preventing cu oxidation after sintering, Polymers 16 (3) (2024), https://doi.org/10.3390/polym16030398.

[20] T.F. Chen, K.S. Siow, Comparing the mechanical and thermal-electrical properties of sintered copper (Cu) and sintered silver (Ag) joints, J. Alloy. Compd. 866 (2021), https://doi.org/10.1016/j.jallcom.2021.158783.

[21] H.T. Wang, K.B. Yeo, Ieee, Material Analysis and Process Characterization of Super High Thermal Performance Die Attach Epoxy towards Package Reliability, Thermal and Electrical Performance, 35th IEEE/CPMT International Electronic Manufacturing Technology Symposium (IEMT), Ieee, Ipoh, MALAYSIA, 2012.

[22] T. Fukushima, M. Inoue, Control of silver micro-flakes sintering and connection properties of epoxy-based conductive adhesives by the effectiveness of binder chemistry, Materials 18 (2) (2025), https://doi.org/10.3390/ma18020217.

[23] P. Maroulas, D. Dragatogiannis, A. Kyritsis, C. Charitidis, Electrical/thermal conductivities of low-temperature sintered/Ag-decorated epoxy microspheres, Mater. Chem. Phys. 319 (2024), https://doi.org/10.1016/j.matchemphys.2024.129355.

[24] K.P. Yoon, W.K. Kim, The behavioral TOPSIS, Expert Syst. Appl. 89 (2017) 266–272, https://doi.org/10.1016/j.eswa.2017.07.045.

[25] E.K. Zavadskas, A. Mardani, Z. Turskis, A. Jusoh, K.M.D. Nor, Development of TOPSIS method to solve complicated decision-making problems: an overview on developments from 2000 to 2015, Int. J. Inf. Technol. Decis. Mak. 15 (3) (2016) 645–682, https://doi.org/10.1142/s0219622016300019.

[26] M. Akram, W.A. Dudek, F. Ilyas, Group decision-making based on pythagorean fuzzy TOPSIS method, Int. J. Intell. Syst. 34 (7) (2019) 1455–1475, https://doi.org/10.1002/int.22103.

[27] Y. Celikbilek, F. Tuysuz, An in-depth review of theory of the TOPSIS method: an experimental analysis, J. Manag. Anal. 7 (2) (2020) 281–300, https://doi.org/10.1080/23270012.2020.1748528.

[28] J.H. Su, Y.D. Sun, An improved TOPSIS model based on cumulative prospect theory: application to ESG performance evaluation of State-Owned mining enterprises, Sustainability 15 (13) (2023) 20, https://doi.org/10.3390/su151310046.

[29] C. Wang, J.X. Shi, Y. Yang, R. Wang, Two methods with bidirectional similarity for optimal selections of supplier portfolio and supplier substitute based on TOPSIS and IFS, IEEE Access 12 (2024) 1761–1773, https://doi.org/10.1109/access.2023.3348522.

[30] A. Fahmi, A. Khan, T. Abdeljawad, M.A. Alqudah, Natural gas based on combined fuzzy TOPSIS technique and entropy, Heliyon 10 (1) (2024) 16, https://doi.org/10.1016/j.heliyon.2023.e23391.

[31] M. Akram, C. Kahraman, K. Zahid, Extension of TOPSIS model to the decision-making under complex spherical fuzzy information, Soft Comput. 25 (16) (2021) 10771–10795, https://doi.org/10.1007/s00500-021-05945-5.

[32] K.-H. Jung, K.D. Min, C.-J. Lee, B.-G. Park, H. Jeong, J.-M. Koo, B. Lee, S.-B. Jung, Effect of epoxy content in ag nanoparticle paste on the bonding strength of MLCC packages, Appl. Surf. Sci. 495 (2019), https://doi.org/10.1016/j.apsusc.2019.07.229.

[33] X. Wang, Z. Zeng, G. Zhang, J. Zhang, P. Liu, Joint analysis and reliability test of Epoxy-Based nano silver paste under different Pressure-Less sintering processes, J. Electron. Packag. 144 (4) (2022), https://doi.org/10.1115/1.4053432.

[34] B.-U. Hwang, K.-H. Jung, K.D. Min, C.-J. Lee, S.-B. Jung, Pressureless Cu–Cu bonding using hybrid Cu–epoxy paste and its reliability, J. Mater. Sci. Mater. Electron. 32 (3) (2021) 3054–3065, https://doi.org/10.1007/s10854-020-05055-2.